Minireview

Towards clinical photoacoustic and ultrasound imaging: Probe improvement and real-time graphical user interface

Jeesu Kim*, Eun-Yeong Park*, Byullee Park, Wonseok Choi, Ki J Lee and Chulhong Kim

Departments of Creative IT Engineering, Electrical Engineering, and Mechanical Engineering, Pohang University of Science and Technology (POSTECH), Gyeongbuk 37673, Republic of Korea

*These authors contributed equally to this work.

Corresponding author: Chulhong Kim. Email: chulhong@postech.edu

Impact statement

Photoacoustic imaging is a promising biomedical imaging modality that can visualize both structural and functional information of biological tissue. Because of its easiness to be integrated with conventional ultrasound imaging systems, numerous studies have been conducted to develop and apply clinical photoacoustic imaging systems. However, most of the systems were not suitable for general-purpose clinical applications due to one of the following reasons: target specific design, immobility, inaccessible operation sequence, and lack of hand-held operation. This study demonstrates a real-time clinical photoacoustic and ultrasound imaging system, which can overcome the limitations of the previous systems for successful clinical translation.

Abstract

Photoacoustic imaging is a non-invasive and non-ionizing biomedical technique that has been investigated widely for various clinical applications. By taking the advantages of conventional ultrasound imaging, hand-held operation with a linear array transducer should be favorable for successful clinical translation of photoacoustic imaging. In this paper, we present new key updates contributed to the previously developed real-time clinical photoacoustic and ultrasound imaging system for improving the clinical usability of the system. We developed a seamless image optimization platform, designed a real-time parameter control software with a user-friendly graphical user interface, performed Monte Carlo simulation of the optical fluence in the imaging plane, and optimized the geometry of the imaging probe. The updated system allows optimizing of all imaging parameters while continuously acquiring the photoacoustic and ultrasound images in real-time. The updated system has great potential to be used in a variety of clinical applications such as assessing the malignancy of thyroid cancer, breast cancer, and melanoma.

Keywords: Clinical system, real-time imaging, photoacoustic imaging, ultrasound imaging, seamless parameter optimization, imaging probe optimization

Experimental Biology and Medicine **2020; 245: 321–329. DOI: 10.1177/1535370219889968**

Introduction

Photoacoustic (PA) imaging is a non-invasive biomedical imaging modality that has gained great interest in a variety of clinical and preclinical applications. The principle of PA imaging is based on the PA effect, which is energy transduction from light to ultrasound (US) waves.[1] The strength of PA imaging is in its ability to visualize the optical absorption characteristics of biological tissues at US resolution in relatively deep tissues.[2–4] The PA imaging also provides functional information[5–8] as well as molecular information of biological tissue by using exogenous contrast agents.[9–17] Thanks to the combination of optical and US imaging techniques, PA imaging overcomes the associated drawbacks of each modality achieving much deeper imaging depth compared to pure optical imaging and enhanced optical contrast compared to US imaging.

PA imaging has several unique advantages for clinical applications: (1) PA imaging can be easily integrated into a conventional clinical US machine because the signal receiving and image generation procedure of these two modalities are similar.[18–24] The dual-modal PA/US images provide complementary information for accurate diagnoses. (2) PA imaging enables visualization of a vasculature network because the hemoglobin in the blood vessel is a strong optical absorber.[25–31] Compared to conventional angiographic techniques such as X-ray computed tomography (CT) and

magnetic resonance imaging (MRI), PA imaging does not require any exogenous contrast agent, thus avoiding the side effects of contrast agents.[32] (3) By analyzing multispectral PA images, the chemical composition of biological tissues can be described using the spectral unmixing method.[33–38] Exploiting the advantages described above, various clinical studies using PA imaging systems have been conducted.[39–46]

We previously developed a real-time clinical PA and US imaging system based on a general-purpose US machine. The main feature of this system is the programmable architecture, which allows the user to modify the operation sequence of the system.[47–50] By modifying the operation sequence of the US machine, we were able to display PA, US, and overlaid PAUS images in real-time. The system showed great potential as a research tool for various clinical applications with several advantages, including real-time imaging capability, intuitive user interface, hand-held operation, and portability. Two important features not addressed in the previous system were: optimal probe design to deliver light efficiently for better signal-to-noise ratio (SNR) and the general-purpose clinical tool to allow real-time modification of the imaging parameters.

Here, we present our new clinical PA and US imaging system. The updated system provides seamless optimization of imaging parameters during real-time visualization of PA and US images. The design of the integrated PA and US imaging probe is also updated for efficient light delivery. Since our system is based upon an FDA-cleared general-purpose US machine, the system can be used readily in the clinical field. In addition, the programmability of the US machine enables the system to be applied in a variety of clinical and preclinical studies.

Real-time clinical photoacoustic and ultrasound imaging system

Previously, we developed a real-time clinical PA and US imaging system by synchronizing a tunable mobile laser (Phocus Mobile, OPOTEK, USA) with a programmable US machine (EC12R, Alpinion Medical Systems, Republic of Korea) (Figure 1). In brief, an optical parametric oscillator (OPO) laser pumped by an Nd:YAG laser generates a wavelength-tunable pulsed laser beam, which is delivered by a bifurcated fiber bundle integrated with a linear array US transducer (L3-12, Alpinion Medical Systems, Republic of Korea). The design of the bifurcated fiber bundles is shown in Figure S1. Each branch of fiber bundle has one layer of 248 fibers (core diameter of 176 μm). The fibers are uniformly distributed over a line of 50 mm along the lateral axis of the transducer. The US and PA signals are received by the data acquisition (DAQ) module and corresponding images are reconstructed using parallel computing available through the graphics processing unit (GPU). The overlaid PA and US images are displayed on the screen in real-time. The system also exports the acquired raw data for further processing.

Modified operation sequence for seamless optimization of imaging parameters

Although the previously developed PA and US imaging system has been used successfully for clinical research but has limitations. The imaging parameters cannot be changed during real-time imaging experiments while using this system (Figure 2(a)). To make any changes in imaging parameters, the image acquisition needs to be terminated, and the operation sequence of the system should be recompiled with the modified parameters. The imaging is then resumed with the modified parameter file. These series of processes take several minutes, which is not practical for clinical studies. For successful clinical outcomes, the seamless modification of the imaging parameters is essential. This limitation in the parameter modification is mainly due to the parameter loading mechanism of the imaging software. The system loads all the imaging parameters in the initialization step, then uses

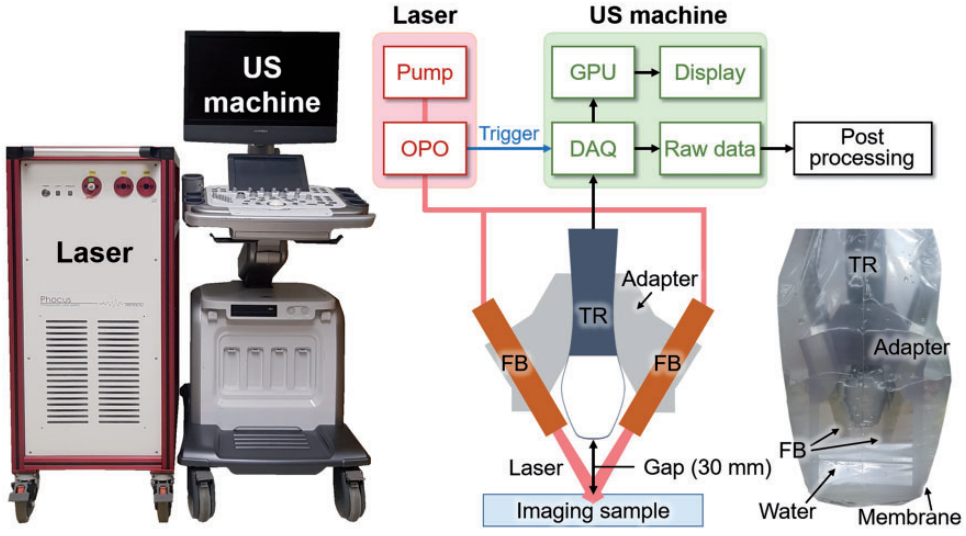

Figure 1. Schematic and photograph of the real-time PA and US imaging system and the integrated imaging probe. The inset is a photograph of the imaging probe. PA: photoacoustic; US: ultrasound; OPO: optical parametric oscillator; DAQ: data acquisition; GPU: graphics processing unit; TR: transducer; FB: fiber bundle. (A color version of this figure is available in the online journal.)

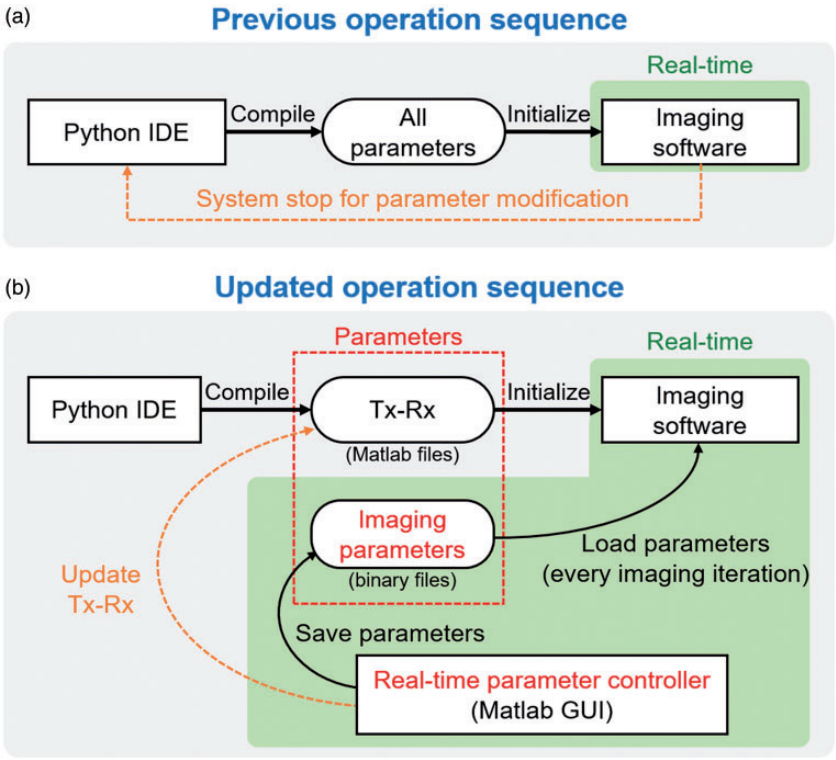

Figure 2. Previous (a) and updated (b) operation sequence for parameter modification in the ultrasound machine. Green boxes denote real-time operations. IDE: independent development environment; Tx: transmission; Rx: reception; GUI: graphical user interface. (A color version of this figure is available in the online journal.)

them for the subsequent imaging process. To accommodate seamless parameter modification, we modify the operation sequence to bypass the parameter initialization procedure (Figure 2(b)). Instead of storing all the parameters in a single file, we separate the transmitting and receiving parameters (Tx-Rx) from imaging parameters and save them as external binary files. In the new format, only Tx-Rx operation is determined in the initialization step, which is similar to the previous operation. The rest of the parameters used for image optimizations are updated at every image acquisition. The main controller of seamless parameter update is custom-made in Matlab (Figure 3). The software receives the modified imaging parameters through a graphical user interface (GUI) and saves the parameters as a series of external binary files. These binary files are loaded repeatedly by the imaging software during the real-time operation (Figure S2). The imaging parameter is divided into five sections based on the functionality (red inset in Figure 3): (1) time gain compensation (TGC) coefficients, (2) beamforming parameters including beamforming method, windowing method, speed of sound, and delay offset, (3) frequency demodulation parameters including demodulation method, center frequency, and cut-off frequency, (4) dynamic range for log compression, and (5) display options. We implement these functional blocks on the GPU for real-time imaging. We can easily compare the generated image quality in real-time and select the best imaging parameter, similar to the optimization process of conventional real-time US imaging systems. Our system also allows switching various beamformers such as delay-and-sum, delay-multiply-and-sum, p-th root compression, and Fourier reconstruction. The software can also modify the Tx-Rx operation by using an additional GUI (blue inset in Figure 3). However, we have to restart the imaging software to apply the modified Tx-Rx operation since the Tx-Rx operation of US machine can only be updated in the initialization step. For post-processing, the raw data of PA and US images are saved in the preset folder, whose data path is set in the control software (green inset in Figure 3). With the modified operation sequence, we can easily optimize the images by constantly monitoring the resulting images via parameter modification.

Improved hand-held probe for photoacoustic and ultrasound imaging

To acquire the PA and US images with the hand-held device, we have designed an adapter to integrate the US transducer and fiber bundle (Figure 1). Before designing the adapter, we simulated the optical fluence in biological tissues using the Monte Carlo simulation tool under various conditions of the laser beam (Figure 4(a)).[51,52] The laser beam distribution was set to mimic the fiber bundle that we used in the system (one layer of 248 fibers in 50 mm for each branch). We controlled two parameters for simulation: incidence angle of the laser beam (θ) and the distance between the laser beam and the imaging plane (i.e. the center axis) at the surface of the imaging sample (Δd). In the Monte Carlo simulation, we generated and tracked one million photon packets in the biological tissue with an absorption

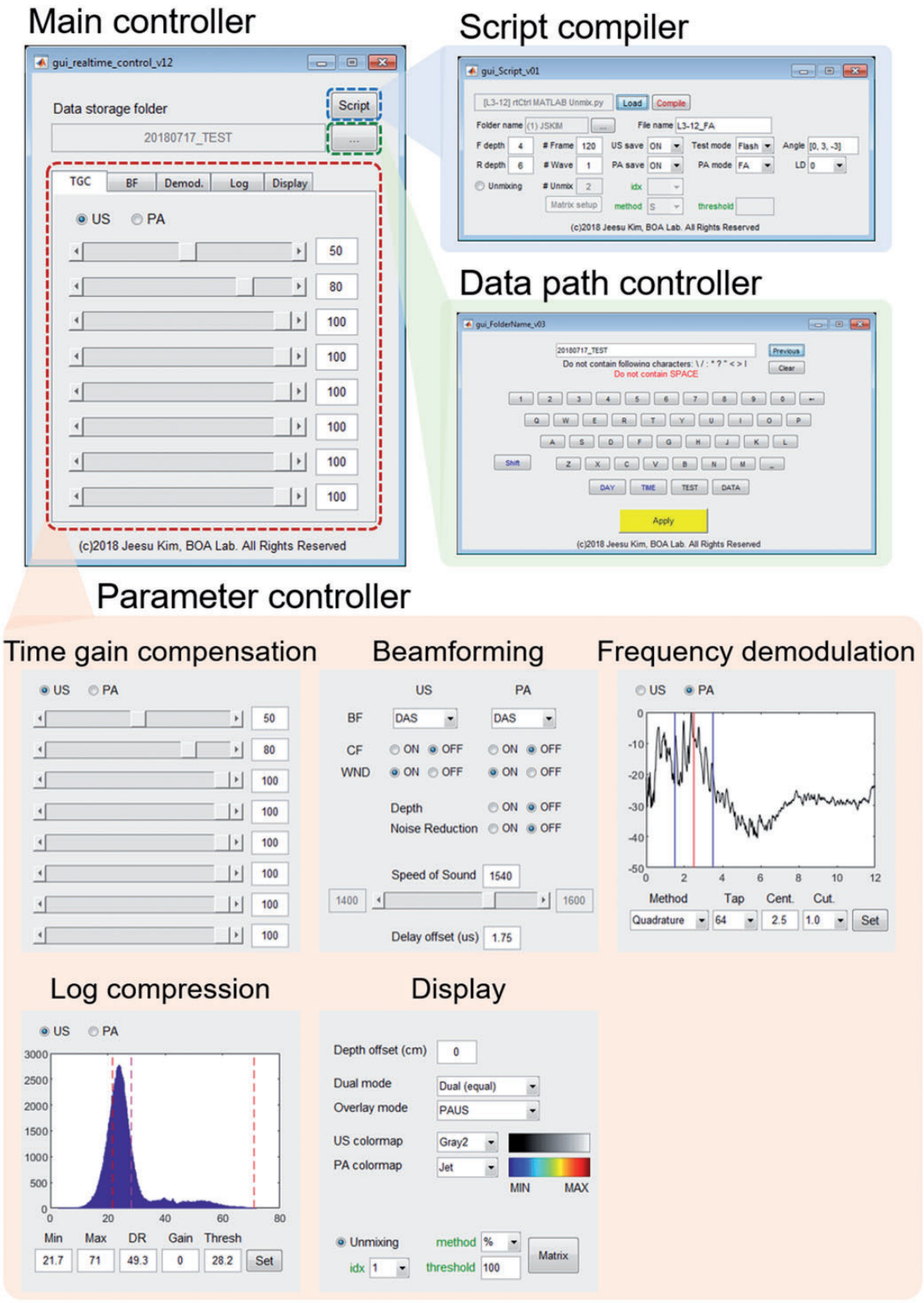

Figure 3. Real-time parameter control software based on the MATLAB platform. (A color version of this figure is available in the online journal.)

coefficient of 0.1 cm^{-1}, a scattering coefficient of 100 cm^{-1}, a refractive index of 1.37, and anisotropy of 0.9. We visualized the optical fluence at the imaging plane (Figure S3). By comparing the simulation results from various θ (Figure 4(b)) and various Δd (Figure 4(c)), we found that Δd is the dominant parameter for determining the optical fluence in the imaging plane. Contrary to our initial assumption, the incident angle of the laser beam does not

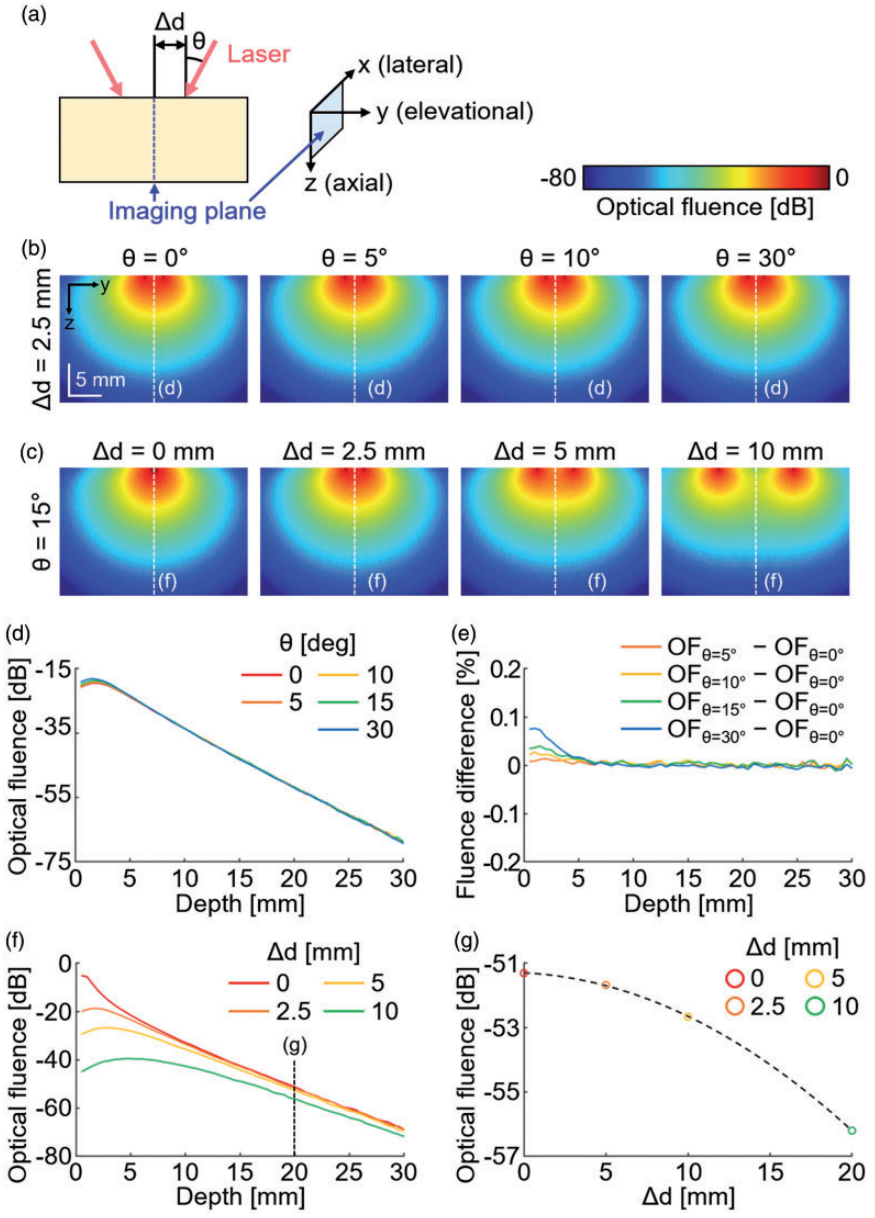

Figure 4. Monte Carlo simulation of light propagation in biological tissues. (a) The illustration of the imaging plane and the incident laser beam. Monte Carlo simulation of optical fluence in biological tissues with the fixed distance (b) and fixed angle (c) of the two incident laser beam. (d) Optical fluence at the imaging plane with a fixed distance (5 mm) and various incident angles. (e) Percentile difference in optical fluence at each angle compared to optical fluence at the normal incident ($\theta = 0$). (f), Optical fluence at the imaging plane with a fixed angle (15°) and various distances. (g) Optical fluence at the depth of 20 mm with the various distances between the laser beams. θ: the incident angle of the laser beam; Δd: the distance between two laser beams at the imaging surface; OF: optical fluence. (A color version of this figure is available in the online journal.)

affect the direction of the propagation in deep tissue (Figure 4(d)). Compared to the normal incidence, the percentile difference in optical fluence at each angle is less than 0.1% (Figure 4(e)). In contrast, the optical fluence significantly decreases as the Δd increases (Figure 4(f)). At the imaging depth of 20 mm, which is the typical imaging depth of human tissue, the optical fluences at the center of the imaging plane are compared with various Δd (Figure 4(g)). The optical fluence with $\Delta d = 0$ mm is ~5 dB higher than the optical fluence with $\Delta d = 10$ mm, which was used in the previous imaging probe (Figure S4). Based on the findings from simulation, we designed the adapter to bring the laser beam as close as possible to the sample surface. The adapter was designed using a 3D design software (Inventor, Autodesk, USA) and implemented using a 3D printer (ProJet MJP 2500, 3 D SYSTEMS, USA). To shorten the Δd, we added a stand-off between the US transducer and the sample due to the thickness of the fiber bundle. With the stand-off, reflection artifacts originated from the PA waves at the transducer surface were present at twice the distance of the gap (Figure S5). To avoid the reflection artifacts, we set the thickness of the stand-off as 30 mm, which is more than the PA imaging depth in human tissues. We sealed the integrated imaging probe using a membrane (Safety Lock, Eraesi, Republic of Korea) and used water as the medium

of transmission. The transparency of the US membrane is certified since it is used conventionally in clinical US imaging during surgical operations. The same membrane is also available for PA imaging due to its optical transparency of ~95% (Figure S6).

In vitro phantom experiments

We compared the previously designed and the currently updated imaging probe by quantifying PA and US signals of the phantom *in vitro*. We prepared chicken breast tissues and inserted a carbon rod as an imaging target (Figure 5(a)). To match the acoustic impedance between the imaging probe and the phantom, we applied a conventional US gel (Ecosonic, SANIPIA, Republic of Korea) at the region of imaging. The carbon rod is detectable in the PA images from both imaging probes (previous and current) since the color of the carbon rod is black (Figure 5(b)). The US images are displayed in grayscale, and the PA images are displayed in pseudo-color. There are two major differences between the previous and the updated design of the probe (Figure S3): the first is the Δd (10 mm in the previous design, and ~0 mm in the updated design) and the second is the distance between the transducer and the sample surface (0 mm in the previous design and 30 mm in the updated design). The previous Monte Carlo simulation results indicate that the PA SNR would be enhanced with the updated imaging probe, while the US signals might be slightly degraded due to the increased imaging distance. Encouragingly, the *in vitro* results follow our readout (Figure 5(c)). The PA SNR acquired with the updated probe is enhanced by ~7 dB compared to the previous probe, which matches with the Monte Carlo simulation results. The US SNR is slightly decreased, but the difference is minimal. We can also note that the PA SNR is much higher than the US SNR because there is no background signal in the PA images, while the US images have speckle patterns from the background tissues.

Parameter-optimized real-time photoacoustic and ultrasound imaging of a human volunteer

To evaluate the updated system *in vivo*, we acquired PA and US images of a human volunteer (Figure 6). We recruited a volunteer and acquired images in the neck area. All the recruiting and data acquisition followed the protocol that is approved by the institutional review board of Pohang University of Science and Technology (POSTECH). During the image acquisition, we were able to modify the imaging parameters to optimize the image by using the

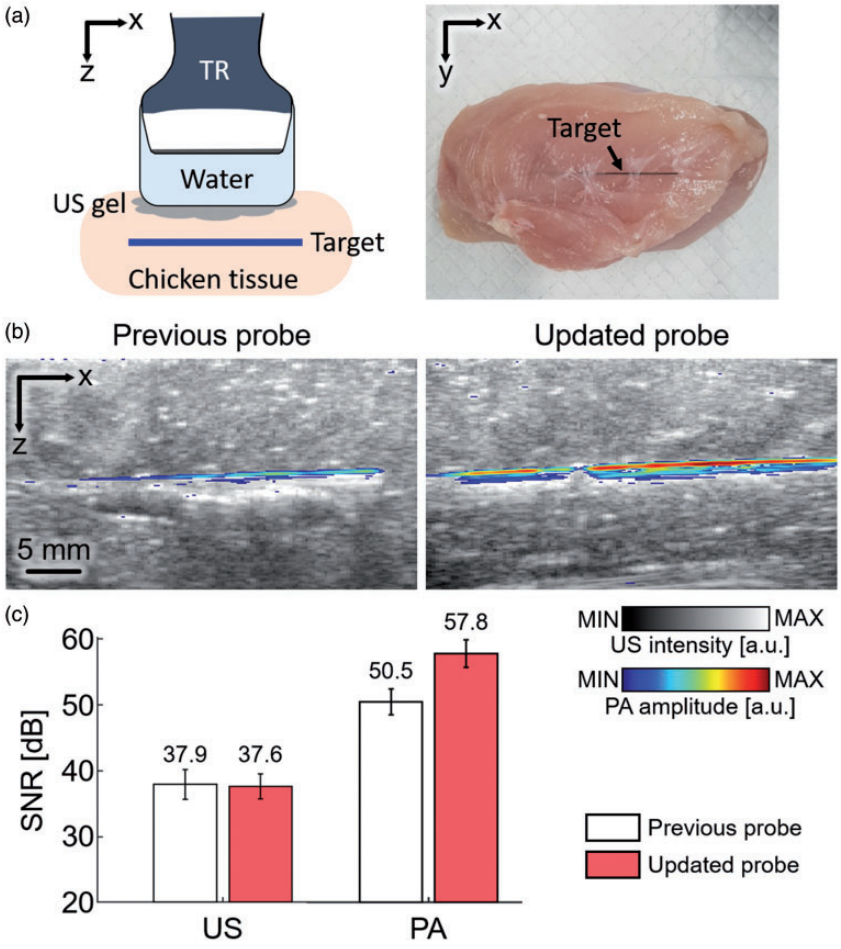

Figure 5. PA and US imaging of a phantom with the integrated imaging probe. (a) The schematic and a photograph of the phantom. (b) Overlaid PA and US images of the phantom by using the previous and the updated imaging probes. (c) Quantification results of the SNR from the PA and US signals of the imaging target. PA: photoacoustic; US: ultrasound; TR: transducer; SNR: signal-to-noise ratio. (A color version of this figure is available in the online journal.)

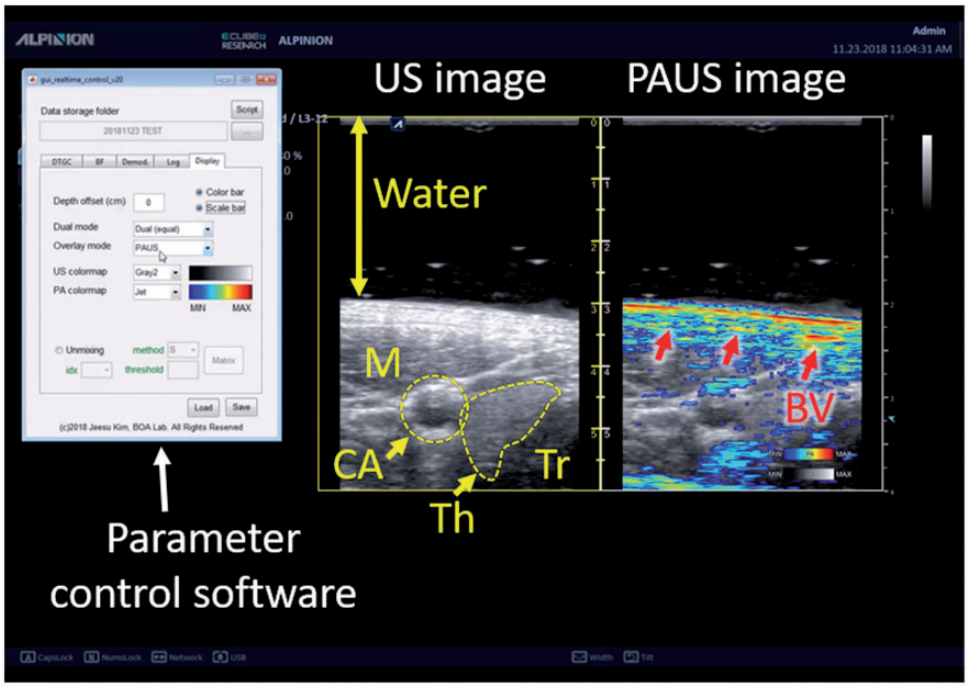

Figure 6. Captured PA and US image from the US machine during real-time imaging of human *in vivo*. PA: photoacoustic; US: ultrasound; M: muscle; CA: carotid artery; Th: thyroid; Tr: Trachea; BV: blood vessel. (A color version of this figure is available in the online journal.)

parameter control software without pausing the imaging operation (Movie S1). Similar to conventional US imaging machines, we can adjust time gain compensation coefficients and dynamic range for image optimization. We can also modify the beamforming options (beamforming method, apodization window type, and speed of sound) and the demodulation frequencies (center frequency, cutoff frequency, and filter size) to optimize images. In addition, various display options including colormap selection, axis visualization, and single/dual display mode make the system easy to use by users who are familiar with conventional US machines. In the US images, internal structures including carotid artery, thyroid lobe, trachea, and neck muscles are visible. On the other hand, the PA images display the optical absorption characteristics of tissues. Since we did not inject any contrast agent, most of the PA signals are generated from blood vessels due to the strong optical absorption of the hemoglobin. In addition to the carotid artery, which generates strong PA signals, small superficial blood vessels are also visible in the PA images (Red arrows in Figure 6).

Discussion and conclusion

In this paper, we demonstrate a novel clinical PA and US imaging system, which supports real-time parameter modification during imaging. Using the parameter control platform, the user can easily modify parameters for optimizing real-time images. We also optimized laser delivery to achieve better PA SNR and developed an adapter to attach the fiber bundle to the hand-held PA and US imaging probe. Table S1 shows the quantitative comparison between the previously reported and currently updated systems. Compared to the previously reported system, the currently updated system allows the user to modify imaging parameters without terminating the operation. The user-friendly GUI also helps the user to optimize the images. The updated imaging probe is slightly bigger than the previous one but produces better PA SNR while maintaining US SNR. The updated system is highly translatable to the clinical field because (1) the US machine is cleared by FDA, (2) the sequence-programming and parameter-optimization platform enable the clinician to use the system for any clinical application, (3) all the data acquisition and image generation processes are performed in real-time, and (4) the entire system is portable. The developed system can be used to provide new biological information in diagnostic fields such as thyroid cancer, breast cancer, and skin cancer. In addition, due to the system's excellent ability to visualize blood vessel networks without injecting any contrast agent, it can also be used for assessing peripheral vasculature disease, monitoring angiogenesis, and measuring inflammation. Thus, our system advances PA imaging one more step towards the translation clinical use.

Authors' contributions: All authors participated in the design, interpretation of the studies and analysis of the data and review of the manuscript; JK and CK designed all the experiments, interpreted the results, and wrote the manuscript, JK designed and implemented the seamless parameter optimization platform, JK, EYP, WC, and KJL designed and implemented customized functional blocks for real-time image generation, JK and EYP simulated optical fluence in biological tissue to optimize the probe design, JK and BP designed, implemented, and tested the hand-held probe.

DECLARATION OF CONFLICTING INTERESTS

The author(s) declared the following potential conflicts of interest with respect to the research, authorship, and/or publication of this article: Chulhong Kim and Ki Jong Lee have financial interests in OPTICHO, which, however, did not support this work.

FUNDING

The author(s) disclosed receipt of the following financial support for the research, authorship, and/or publication of this article: This research was supported by the MSIP (Ministry of Science, ICT and Future Planning), Korea, under the "ICT Consilience Creative Program" (IITP-2019–2011-1–00783), supervised by the IITP (Institute for Information & Communications Technology Promotion). It was also supported by the Pioneer Research Center Program (2017M3C1A3037762), and the Basic Science Research Programs (NRF-2019R1A2C2006269, 2018R1A6A3A01011442) through the National Research Foundation of Korea funded by the Ministry of Education.

ORCID iD

Chulhong Kim https://orcid.org/0000-0001-7249-1257

SUPPLEMENTAL MATERIAL

Supplemental material for this article is available online.

REFERENCES

1. Bell AG. The photophone. *Science* 1880;**1**:130–1
2. Kim C, Favazza C, Wang LV. In vivo photoacoustic tomography of chemicals: high-resolution functional and molecular optical imaging at new depths. *Chem Rev* 2010;**110**:2756–82
3. Wang LV, Hu S. Photoacoustic tomography: in vivo imaging from organelles to organs. *Science* 2012;**335**:1458–62
4. Jeon S, Kim J, Lee D, Woo BJ, Kim C. Review on practical photoacoustic microscopy. *Photoacoustics* 2019;**15**:100141
5. Wang X, Stoica G, Xie X, Ku G, Wang LV. Noninvasive imaging of hemoglobin concentration and oxygenation in the rat brain using high-resolution photoacoustic tomography. *J Biomed Opt* 2006;**11**:024015–9
6. Zhang HF, Maslov K, Sivaramakrishnan M, Stoica G, Wang LV. Imaging of hemoglobin oxygen saturation variations in single vessels in vivo using photoacoustic microscopy. *Appl Phys Lett* 2007;**90**:053901
7. Lee C, Jeon M, Jeon MY, Kim J, Kim C. In vitro photoacoustic measurement of hemoglobin oxygen saturation using a single pulsed broadband supercontinuum laser source. *Appl Opt* 2014;**53**:3884–9
8. Yao J, Maslov KI, Shi Y, Taber LA, Wang LV. In vivo photoacoustic imaging of transverse blood flow by using Doppler broadening of bandwidth. *Opt Lett* 2010;**35**:1419–21
9. Zhang Y, Jeon M, Rich LJ, Hong H, Geng J, Zhang Y, Shi S, Barnhart TE, Alexandridis P, Huizinga JD. Non-invasive multimodal functional imaging of the intestine with frozen micellar naphthalocyanines. *Nat Nanotech* 2014;**9**:631–8
10. Lee C, Kim J, Zhang Y, Jeon M, Liu C, Song L, Lovell JF, Kim C. Dual-color photoacoustic lymph node imaging using nanoformulated naphthalocyanines. *Biomaterials* 2015;**73**:142–8
11. Lee MY, Lee C, Jung HS, Jeon M, Kim KS, Yun SH, Kim C, Hahn SK. Biodegradable photonic melanoidin for theranostic applications. *ACS Nano* 2016;**10**:822–31
12. Song J, Kim J, Hwang S, Jeon M, Jeong S, Kim C, Kim S. Smart gold nanoparticles for photoacoustic imaging: an imaging contrast agent responsive to the cancer microenvironment and signal amplification via pH-induced aggregation. *Chem Commun* 2016;**52**:8287–90
13. Park S, Park G, Kim J, Choi W, Jeong U, Kim C. Bi2Se3 nanoplates for contrast-enhanced photoacoustic imaging at 1064 nm. *Nanoscale* 2018;**10**:20548–58
14. Jung H, Park S, Gunassekaran GR, Jeon M, Cho Y-E, Baek M-C, Park JY, Shim G, Oh Y-K, Kim I-S, Kim C, Lee B. A peptide probe enables photoacoustic-guided imaging and drug delivery to lung tumors in K-rasLA2 mutant mice. *Cancer Res* 2019;doi: 10.1158/0008-5472.CAN-18-3089
15. Jeon M, Song W, Huynh E, Kim J, Kim J, Helfield BL, Leung BY, Goertz DE, Zheng G, Oh J. Methylene blue microbubbles as a model dual-modality contrast agent for ultrasound and activatable photoacoustic imaging. *J Biomed Opt* 2014;**19**:016005
16. Akers WJ, Edwards WB, Kim C, Xu B, Erpelding TN, Wang LV, Achilefu S. Multimodal sentinel lymph node mapping with single-photon emission computed tomography (SPECT)/computed tomography (CT) and photoacoustic tomography. *Transl Res* 2012;**159**:175–81
17. Xia J, Kim CF, Lovell J. Opportunities for photoacoustic-guided drug delivery. *Curr Drug Targets* 2015;**16**:571–81
18. Kim J, Park S, Jung Y, Chang S, Park J, Zhang Y, Lovell JF, Kim C. Programmable real-time clinical photoacoustic and ultrasound imaging system. *Sci Rep* 2016;**6**:35137
19. Kim C, Erpelding TN, Jankovic L, Pashley MD, Wang LV. Deeply penetrating in vivo photoacoustic imaging using a clinical ultrasound array system. *Biomed Opt Exp* 2010;**1**:278–84
20. Erpelding TN, Kim C, Pramanik M, Jankovic L, Maslov K, Guo Z, Margenthaler JA, Pashley MD, Wang LV. Sentinel lymph nodes in the rat: noninvasive photoacoustic and US imaging with a clinical US system 1. *Radiology* 2010;**256**:102–10
21. Kim C, Erpelding TN, Jankovic L, Wang LV. Performance benchmarks of an array-based hand-held photoacoustic probe adapted from a clinical ultrasound system for non-invasive sentinel lymph node imaging. *Proc R Soc A* 2011;**369**:4644–50
22. Xia J, Wei C-w, Nguyen T-M, Arnal B, Pelivanov I, M O'Donnell, editors. Clinically translatable integrated ultrasound and photoacoustic imaging system. *SPIE BiOS* 2014;**8943**:894310
23. Asao Y, Hashizume Y, Suita T, Nagae K-I, Fukutani K, Sudo Y, Matsushita T, Kobayashi S, Tokiwa M, Yamaga I. Photoacoustic mammography capable of simultaneously acquiring photoacoustic and ultrasound images. *J Biomed Opt* 2016;**21**:116009
24. Jeon M, Kim C. Multimodal photoacoustic tomography. *IEEE Trans Multimedia* 2013;**15**:975–82
25. Wang Y, Wang D, Hubbell R, Xia J. Second generation slit-based photoacoustic tomography system for vascular imaging in human. *J Biophotonics* 2017;**10**:799–804
26. Irisawa K, Hirota K, Hashimoto A, Murakoshi D, Ishii H, Tada T, Wada T, Hayakawa T, Hayakawa R, Otani N, editors. Photoacoustic imaging system for peripheral small-vessel imaging based on clinical ultrasound technology. *Photons Plus Ultrasound* 2016;**9708**:970807
27. Taruttis A, Timmermans AC, Wouters PC, Kacprowicz M, van Dam GM, Ntziachristos V. Optoacoustic imaging of human vasculature: feasibility by using a handheld probe. *Radiology* 2016;**281**:256–63
28. Wang D, Wang Y, Wang W, Luo D, Chitgupi U, Geng J, Zhou Y, Wang L, Lovell JF, Xia J. Deep tissue photoacoustic computed tomography with a fast and compact laser system. *Biomed Opt Exp* 2017;**8**:112–23
29. Kitai T, Torii M, Sugie T, Kanao S, Mikami Y, Shiina T, Toi M. Photoacoustic mammography: initial clinical results. *Breast Cancer* 2014;**21**:146–53
30. Kruger RA, Lam RB, Reinecke DR, Del Rio SP, Doyle RP. Photoacoustic angiography of the breast. *Med Phys* 2010;**37**:6096–100
31. Baik JW, Kim JY, Cho S, Choi S, Kim J, Kim C. Super wide-field photoacoustic microscopy of animals and humans in vivo. *IEEE Transac Med Imag* 2019;10.1109/TMI.2019.2938518
32. Laskey W, Aspelin P, Davidson C, Rudnick M, Aubry P, Kumar S, Gietzen F, Wiemer M, Group DS. Nephrotoxicity of iodixanol versus iopamidol in patients with chronic kidney disease and diabetes mellitus undergoing coronary angiographic procedures. *Am Heart J* 2009;**158**:822–8.e3

33. Luís Deán-Ben X, Razansky D. Adding fifth dimension to optoacoustic imaging: volumetric time-resolved spectrally enriched tomography. *Light Sci Appl* 2014;**3**:e137
34. Dima A, Burton NC, Ntziachristos V. Multispectral optoacoustic tomography at 64, 128, and 256 channels. *J Biomed Opt* 2014;**19**:036021
35. Glatz J, Deliolanis NC, Buehler A, Razansky D, Ntziachristos V. Blind source unmixing in multi-spectral optoacoustic tomography. *Opt Exp* 2011;**19**:3175–84
36. Kim J, Kim Y, Park B, Seo H, Bang C, Park G, Park Y, Rhie J, Lee J, Kim C. Multispectral ex vivo photoacoustic imaging of cutaneous melanoma for better selection of the excision margin. *Br J Dermatol* 2018;**179**:780–82
37. Knieling F, Neufert C, Hartmann A, Claussen J, Urich A, Egger C, Vetter M, Fischer S, Pfeifer L, Hagel A. Multispectral optoacoustic tomography for assessment of Crohn's disease activity. *N Engl J Med* 2017;**376**:1292–4
38. Li M, Tang Y, Yao J. Photoacoustic tomography of blood oxygenation: a mini review. *Photoacoustics* 2018;**10**:65–73
39. Choi W, Park E-Y, Jeon S, Kim C. Clinical photoacoustic imaging platforms. *Biomed Eng Lett* 2018;**8**:1–17
40. Lin L, Hu P, Shi J, Appleton CM, Maslov K, Li L, Zhang R, Wang LV. Single-breath-hold photoacoustic computed tomography of the breast. *Nat Commun* 2018;**9**:2352
41. Toi M, Asao Y, Matsumoto Y, Sekiguchi H, Yoshikawa A, Takada M, Kataoka M, Endo T, Kawaguchi-Sakita N, Kawashima M. Visualization of tumor-related blood vessels in human breast by photoacoustic imaging system with a hemispherical detector array. *Sci Rep* 2017;**7**:41970
42. Horiguchi A, Tsujita K, Irisawa K, Kasamatsu T, Hirota K, Kawaguchi M, Shinchi M, Ito K, Asano T, Shinmoto H. A pilot study of photoacoustic imaging system for improved real-time visualization of neurovascular bundle during radical prostatectomy. *Prostate* 2016;**76**:307–15
43. Wang X, Jo J, Xu G, Marquardt A, Francis S, Gandikota G, Yuan J, editors. Photoacoustic imaging of human inflammatory arthritis. In: *IEEE international ultrasonics symposium (IUS)*, Taipei, 21 October 2015, pp.1–4 Piscataway, NJ: IEEE.
44. Neuschler EI, Butler R, Young CA, Barke LD, Bertrand ML, Böhm-Vélez M, Destounis S, Donlan P, Grobmyer SR, Katzen J. A pivotal study of optoacoustic imaging to diagnose benign and malignant breast masses: a new evaluation tool for radiologists. *Radiology* 2017;**287**:398–412
45. Yang M, Zhao L, He X, Su N, Zhao C, Tang H, Hong T, Li W, Yang F, Lin L. Photoacoustic/ultrasound dual imaging of human thyroid cancers: an initial clinical study. *Biomed Opt Exp* 2017;**8**:3449–57
46. Steinberg I, Huland DM, Vermesh O, Frostig HE, Tummers WS, Gambhir SS. Photoacoustic clinical imaging. *Photoacoustics* 2019;**14**:77–98
47. Kim J, Choi W, Park E-Y, Kang Y, Lee KJ, Kim HH, Kim WJ, Kim C. Real-time photoacoustic thermometry combined with clinical ultrasound imaging and high intensity focused ultrasound. *IEEE Transac Biomed Eng*. 10.1109/TBME.2019.2904087
48. Park S, Jang J, Kim J, Kim YS, Kim C. Real-time triple-modal photoacoustic, ultrasound, and magnetic resonance fusion imaging of humans. *IEEE Trans Med Imaging* 2017;**36**:1912–21
49. Kim J, Kim Y, Park B, Seo HM, Bang C, Park G, Park Y, Rhie J, Lee J, Kim C. Multispectral ex vivo photoacoustic imaging of cutaneous melanoma for better selection of the excision margin. *Br J Dermatol* 2018;**179**:780–2
50. Jeon S, Park E-Y, Choi W, Managuli R, Jong Lee K, Kim C. Real-time delay-multiply-and-sum beamforming with coherence factor for in vivo clinical photoacoustic imaging of humans. *Photoacoustics* 2019;**15**:100136
51. Wang L, Jacques SL, Zheng L. MCML—Monte Carlo modeling of light transport in multi-layered tissues. *Comput Meth Programs Biomed* 1995;**47**:131–46
52. Sivasubramanian K, Periyasamy V, Wen KK, Pramanik M. Optimizing light delivery through fiber bundle in photoacoustic imaging with clinical ultrasound system: Monte Carlo simulation and experimental validation. *J Biomed Opt* 2016;**22**:041008